# Calcium-Antimony Alloys as Electrodes for Liquid Metal Batteries

**Takanari Ouchi,[a,*] Hojong Kim,[b,*] Xiaohui Ning,[c] and Donald R. Sadoway[a,*,z]**

[a]*Department of Materials Science and Engineering, Massachusetts Institute of Technology, Cambridge, Massachusetts 02139-4307, USA*
[b]*Department of Materials Science and Engineering, The Pennsylvania State University, University Park, Pennsylvania 16802-4705, USA*
[c]*Center for Advancing Materials Performance from the Nanoscale (CAMP-Nano), State Key Laboratory for Mechanical Behavior of Materials, Xi'an Jiaotong University, Xi'an 710049, People's Republic of China*

The performance of a calcium-antimony (Ca-Sb) alloy serving as the positive electrode in a Ca‖Sb liquid metal battery was investigated in an electrochemical cell, Ca(in Bi) | LiCl-NaCl-$CaCl_2$ | Ca(in Sb). The equilibrium potential of the Ca-Sb electrode was found to lie on the interval, 1.2–0.95 V versus Ca, in good agreement with electromotive force (*emf*) measurements in the literature. During both alloying and dealloying of Ca at the Sb electrode, the charge transfer and mass transport at the interface are facile enough that the electrode potential varies linearly from 0.95 to 0.75 V vs Ca(s) as current density varies from 50 to 500 mA $cm^{-2}$. The discharge capacity of the Ca‖Sb cells increases as the operating temperature increases due to the higher solubility and diffusivity of Ca in Sb. The cell was successfully cycled with high coulombic efficiency (~100%) and small fade rate (<0.01% $cycle^{-1}$). These data combined with the favorable costs of these metals and salts make the Ca‖Sb liquid metal battery attractive for grid-scale energy storage.
 [DOI: 10.1149/2.0801412jes] 

Manuscript submitted July 17, 2014; revised manuscript received August 25, 2014. Published September 9, 2014.

The liquid metal battery (LMB) has been shown to be an attractive potential solution to the problem of grid-level storage.[1,2] The LMB comprises two liquid metal electrodes separated by a molten salt electrolyte that self-segregate into three liquid layers according to density and immiscibility. In the search for even lower-cost chemistries based on this formula, the Ca-Sb system became the focus of attention because Ca, thanks to its ubiquitous abundance,[3] offers high performance at a low price point. Previous measurements in this laboratory of the thermodynamics of liquid Ca-Sb alloys[4] revealed this system to be high-voltage (0.94–1.04 V) and low-cost (69 \$ $kWh^{-1}$). However, Ca is highly soluble in its salts[5] conferring such a high level of electronic conductivity that a battery fitted with a liquid Ca electrode would exhibit an unacceptably high self-discharge current. In this study we show how to suppress the Ca metal solubility in the molten salt electrolyte so as to make practical a Ca-Sb LMB.

The literature indicates that the solubility of calcium metal is significantly reduced by alloying calcium with other metals to decrease its activity ($a_{Ca}$).[5] Following this, one can envisage a Ca-Sb liquid metal battery as:

$$\text{Ca(in A, } \ell\text{)|electrolyte}(\ell)\text{|Ca(in Sb, } \ell\text{)}, \quad [1]$$

where A is the negative electrode host and the electrolyte can be a solution of molten halide salts with calcium cation as the itinerant. The alloying of calcium with a more noble A metal such as magnesium desirably decreases the melting temperature of the negative electrode, reduces the reactivity of pure calcium metal, and decreases the solubility of calcium in the molten salt electrolyte while undesirably decreasing the cell voltage,[6] albeit an acceptably small amount.

For the cell with Mg as the negative electrode host and Sb as the positive electrode, the half-cell reactions are

$$\text{negative}: \ \text{Ca(in Mg)} = \text{Ca}^{2+} + 2\text{e}^- \quad [2]$$

$$\text{positive}: \ \text{Ca}^{2+} + 2\text{e}^- = \text{Ca(in Sb)} \quad [3]$$

and the resulting overall cell reaction is

$$\text{cell}: \ \text{Ca(in Mg)} = \text{Ca(in Sb)}. \quad [4]$$

On discharge, calcium is electrochemically oxidized out of the negative electrode [Ca(in Mg)→ $Ca^{2+} + 2e^-$]. The $Ca^{2+}$ cations are conducted across the molten salt electrolyte to the positive electrode while electrons are released from the negative current collector to the external circuit. At the positive electrode the $Ca^{2+}$ cations are electrochemically reduced to neutral Ca which dissolves in the metal pool to form a liquid Ca-Sb alloy [$Ca^{2+} + 2e^- \rightarrow$ Ca(in Sb)]. This process is reversed upon charging. The thermodynamic driving force for cell discharge is the difference in chemical potential of Ca between the electrodes,

$$\Delta\bar{G} = \bar{G}_{\text{Ca(in Sb)}} - \bar{G}_{\text{Ca(in Mg)}} \quad [5]$$

where the partial molar Gibbs free energy $\bar{G}_i$ for each component $i$ is given by

$$\begin{aligned}\bar{G}_{\text{Ca(in Sb)}} &= G^{\circ}_{\text{Ca}} + RT\ln a_{\text{Ca(in Sb)}} \\ \bar{G}_{\text{Ca(in Mg)}} &= G^{\circ}_{\text{Ca}} + RT\ln a_{\text{Ca(in Mg)}}\end{aligned} \quad [6]$$

where $a_{Ca}$ is the activity of Ca, $G^{\circ}_{\text{Ca}}$ the standard chemical potential of calcium, $R$ the gas constant, and $T$ the absolute temperature. The difference in partial molar Gibbs free energy can be related to the equilibrium cell voltage, $E_{\text{cell,eq}}$, by the Nernst equation

$$\bar{G}_{\text{cell}} = -zFE_{\text{cell,eq}} \quad [7]$$

where z = 2 is the number of electrons exchanged in the reaction and $F$ is the Faraday constant. From equation 7, the cell equilibrium voltage is related to the activities of calcium in the positive (antimony) and negative (magnesium) electrodes:

$$E_{\text{cell,eq}} = -\frac{\Delta\bar{G}_{\text{cell}}}{zF} = -\frac{RT}{zF}\ln\left(\frac{a_{\text{Ca(in Sb)}}}{a_{\text{Ca(in Mg)}}}\right). \quad [8]$$

With the above equations the equilibrium cell voltage of a Ca-Mg‖Sb cell is estimated to be 0.8–1.02 V, twice the that of a Mg‖Sb cell, 0.39–0.51 V.[1]

In our previous study of Ca-Bi alloys, the dissolution of calcium into molten salt electrolytes was suppressed by a combination of calcium alloying in the electrode and the use of a multi-cation electrolyte.[7] During the course of that work we developed stable reference electrode (RE) and counter electrode (CE), which we have adopted for the present study. The three-electrode electrochemical setup is shown in Figure 1a. As the cell cycles, its voltage deviates from the equilibrium value owing to kinetic limitations including (1) mass transport of Ca in the electrodes, (2) mass transport of $Ca^{2+}$ in the electrolyte, (3) charge transfer at the electrode electrolyte interface, and (4) uncompensated ohmic resistance of the electrolyte, as depicted in Figure 1b.

*Electrochemical Society Active Member.
[z]E-mail: dsadoway@mit.edu

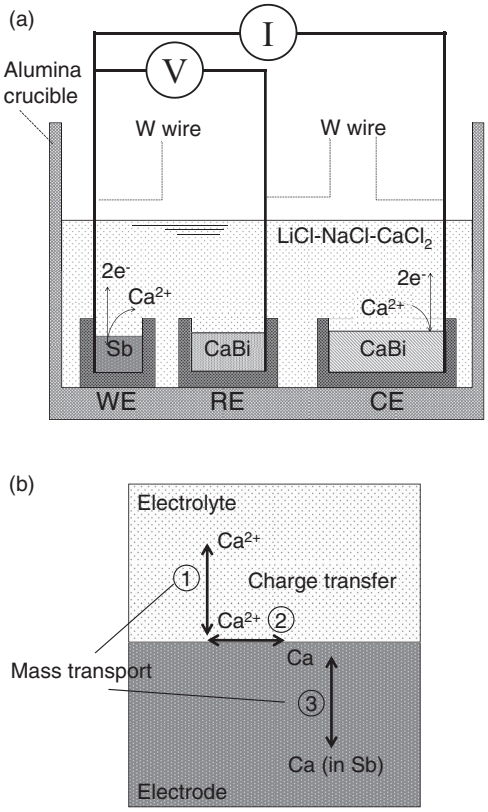


**Figure 1** (a) Electrochemical cell configuration: three-electrode setup comprising the working electrodes (WEs), reference electrodes (REs), and counter electrode (CE). Lead wires are tungsten (W). (b) Schematic illustration of the alloying and dealloying processes at the interface between molten salt and liquid Ca-Sb electrode.

The electrochemical cell of the present study can be represented by

$$\text{Ca(in Bi)|electrolyte|Ca(in Sb)}, \qquad [9]$$

where the electrolyte was a molten salt solution of LiCl-NaCl-$CaCl_2$ (38–27–35 mol%, $T_m = 450°C$). The operating temperature was set at two values: (1) 650°C which exceeds the melting point of antimony ($T_{m,\,Sb} = 630°C$) and (2) 700°C as indicated on the Ca-Sb binary phase diagram (Figure 2).[8] When discharge current flows between the two electrodes, the mole fraction of calcium in antimony, $x_{Ca}$, increases. In

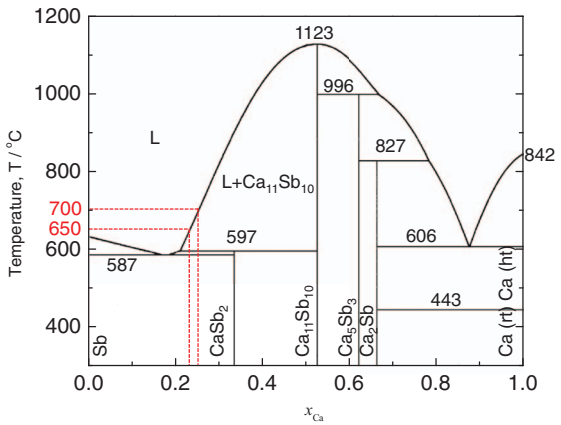


**Figure 2** Phase diagram of Ca-Sb system.[8] Reprinted with permission from ref. 8, Copyright 2006 ASM International.

a three-electrode setup, the voltage is measured between the working electrode (WE) and RE ($E_{cell} = E_{WE} - E_{RE}$) while the current is drawn between WE and CE, as schematically shown in Figure 1a. The RE is a Ca-Bi alloy, $x_{Ca} = 0.35$ (a two phase mixture of solid $Ca_{11}Bi_{10}$ and liquid Bi), chosen due to the invariance of electrode potential with compositional changes within a two-phase regime.[9] The CE is a Ca-Bi alloy, $x_{Ca} = 0.15$ (single liquid phase), which acts as the source of calcium. Assuming negligible polarization of the RE (typically less than ± 2 mV), the WE potential $E_{WE}$ versus Ca(s) can be written as

$$E_{WE} = E_{cell} + E_{RE,eq}, \text{ versus Ca(s)}. \qquad [10]$$

The values of $E_{RE,eq}$ versus Ca(s) are taken from the literature as 0.775 V at 650°C and 0.785 V at 700°C.[10] Moving forward, the following simplified notation for the reported WE potential is used herein: $E_{WE}$ / V versus Ca(s) ≡ $E$ / V, and $E_{WE\,eq}$ / V versus Ca(s) ≡ $E_{eq}$ / V.

## Experimental

*Materials preparation.— Electrodes.—* Pure Sb (99.9999%, Alfa Aesar, Product No. 11071) melted in a boron nitride (BN) crucible (AX05, Saint-Gobain Advanced Ceramics) using an induction heater (MTI Corporation, EQ-SP-15A), installed inside the glove box with an inert argon atmosphere ($O_2$ < 0.1 ppm, $H_2O$ < 0.1 ppm) was prepared as a WE. The dimensions of the BN crucible for the WE were 12 mm in outer diameter, 19 mm in height, 15 mm in depth, 6 mm in inner diameter, and 0.28 $cm^2$ in surface area. CE and RE were prepared from pure Ca (99.99%, Aldrich, Product No. 441872) and Bi (99.999%, Alfa Aesar, Product No. 14442). The CE composed of a Ca-Bi alloy ($x_{Ca} = 0.15$) was also prepared in a BN crucible by induction melting pure Bi and then gradually adding small lumps of Ca metal 2 mm in diameter. The dimensions of the BN crucible for the CE were 25 mm in outer diameter, 22 mm in height, 20 mm in depth, 21 mm in inner diameter, and 3.6 $cm^2$ in surface area. To ensure facile charge transfer kinetics at the CE, its surface area was designed to be over ten times greater than that of the WE. The RE composed of a Ca-Bi alloy ($x_{Ca} = 0.35$) was prepared by arc-melting (MAM1, Edmund Bühler GmbH) pure Ca and Bi metals together to form a homogeneous alloy, which was then transferred to the glove box. There, using an induction heater, the Ca-Bi alloy was re-melted inside BN crucibles. The dimensions of the BN crucible for the RE were 12 mm in outer diameter, 19 mm in height, 15 mm in depth, 8 mm in inner diameter, and 0.50 $cm^2$ in surface area.

*Electrolytes.—*High-purity anhydrous salts of LiCl (99.995%, Alfa Aesar, Product No. 13684), NaCl (99.99%, Alfa Aesar, Product No. 35716), and $CaCl_2$ (99.99%, Alfa Aesar, Product No. 44280) were used to make a 38–27–35 mol% LiCl-NaCl-$CaCl_2$ molten salt solution (m.p. 450°C [7]). The salts were weighed out in appropriate quantities in ∼500 g batches, mixed, and placed into a fused quartz crucible (Technical Glass Products) which was then inserted into a stainless steel vacuum chamber, the chamber sealed, and loaded into a furnace. To prepare dry, homogenous molten salt electrolytes, the test chamber was (1) evacuated to ∼1 Pa, (2) heated at 80°C for 12 h under vacuum, (3) heated at 230°C for 12 h under vacuum, (4) purged with ultra-high purity argon gas (99.999%, $O_2$ < 1 ppm, $H_2O$ < 1 ppm, Airgas Inc.), and (5) heated at 700°C for 3 h under argon gas flowing at 0.2 $cm^3\ s^{-1}$. After cooling to room temperature, the pre-melted electrolyte was transferred back to the glove box and ground into lumps measuring 5–10 mm dia.

*Electrochemical cell assembly.—* The present study was conducted with a three-electrode electrochemical cell assembled in an inert argon atmosphere glove box. Electrical contact with the electrodes was established with tungsten wires (99.95%, Alfa Aesar, Product No. 10411), 1 mm dia., 0.5 m long, which were inserted into each electrode during induction melting. Each electrical lead was insulated from the test vessel by an alumina tube (99.8%, McDanel Advanced Ceramic Technologies). The electrodes were arranged inside an

alumina crucible (99.8%, McDanel Advanced Ceramic Technologies) 56 mm I.D. 100 mm tall and then ~140 g electrolyte was added over them. The final electrochemical cell configuration is shown in Figure 1a. Then the cell was placed within a stainless steel vessel, which was sealed and loaded into a furnace.

*Electrochemical measurements.*— Electrochemical measurements were carried out with a potentiostat-galvanostat (Metrohm AG, PGSTAT302N) and frequency response analyzer (Metrohm AG, FRA32M). For the coulometric titration, alloying and dealloying of Ca with Sb were performed at a current density of 50 mA $cm^{-2}$ for 5450 s, after which time the system was allowed to relax for 5000 s before the equilibrium potential, $E_{eq}$, was recorded. The data were taken only when the potential drift ($dE/dt$) was less than 1 μV $s^{-1}$. The mole fraction of Ca in the WE, $x_{Ca(in\ Sb)}$, was estimated assuming 100% coulombic efficiency. For the evaluation of the rate capability, the potential of the WE was measured as a function of current density during the continuous alloying and dealloying of calcium. Finally, the cycling performance of Ca alloying and dealloying with the Sb electrode was measured with a battery tester (Model 4300, Maccor).

*Characterization.*—The formation of new phases in the positive WE at various stages of discharge (alloying) was investigated by analysis of sectioned specimens by scanning electron microscopy (SEM, JEOL6610), energy dispersive X-ray spectrometry (EDS, IXRF System, Model 55i), and X-ray diffraction (XRD, Bruker D8 multipurpose diffractometer with a GADDS 2D area detector, operated at 40 keV and 40 mA with a copper anode and a 0.5 mm collimator). XRD samples were covered with petroleum jelly to minimize oxidation.

## Results and Discussion

*Determination of thermodynamic properties of Ca-Sb alloy by emf measurements across a molten salt electrolyte.*— To assess the validity of measuring the potential of the Ca-Sb working electrode (WE), $E_{eq}$, in equilibrium with a molten LiCl-NaCl-$CaCl_2$ electrolyte, the composition of calcium in the WE was varied by coulometric titration to values previously studied using a calcium fluoride ($CaF_2$) solid electrolyte[4] in which calcium metal is effectively insoluble.[11]

The variation with composition of the potential of the WE, $E$, and of the current density, $j$, at 650°C is shown in Figure 3a. The values of the equilibrium potential of the WE, $E_{eq}$, plotted as function of mole fraction of calcium in the WE, $x_{Ca(in\ Sb)}$, at 650°C are shown in Figure 3b, which also indicates the liquidus line of the Sb-rich Ca-Sb system.[8] The values of $E_{eq}$ at the sixth and seventh dealloying steps were eliminated because the drift in electrode potential ($dE/dt$) never fell to below 1 μV $s^{-1}$. $E_{eq}$ was also measured at 700°C. Table I compares the values measured herein with those measured previously using a $CaF_2$ solid electrolyte. The values reported from this study are the average of the alloying and dealloying steps. Figure 3 and Table I clearly show that the two studies are in good agreement (differences of ±1–2%). This demonstrates the utility of the multi-cation molten salt electrolyte. The minor differences were considered to be due to the self-discharge current, which will be discussed in more detail below.

*Kinetics of alloying and dealloying of liquid metal in contact with molten salt.*— The operating temperature of the battery is high enough that both electrodes as well as the electrolyte are present in the liquid state. The result is facile charge transfer at the electrode-electrolyte interface[12] and rapid mass transport to and from the electrode-electrolyte interface.[13,14] These features combined with low ohmic losses enabled by the high electrical conductivity of the molten salt electrolytes (up to 3 S $cm^{-1}$) enable the battery to be driven at high charge/discharge rates with small overvoltage. In order to evaluate the kinetics of the alloying and dealloying processes, the potential of the WE, $E$, was measured at current densities of 50, 100, 200, 300, and 500 mA $cm^{-2}$ at 650°C (Figure 4). The equilibrium potentials of the

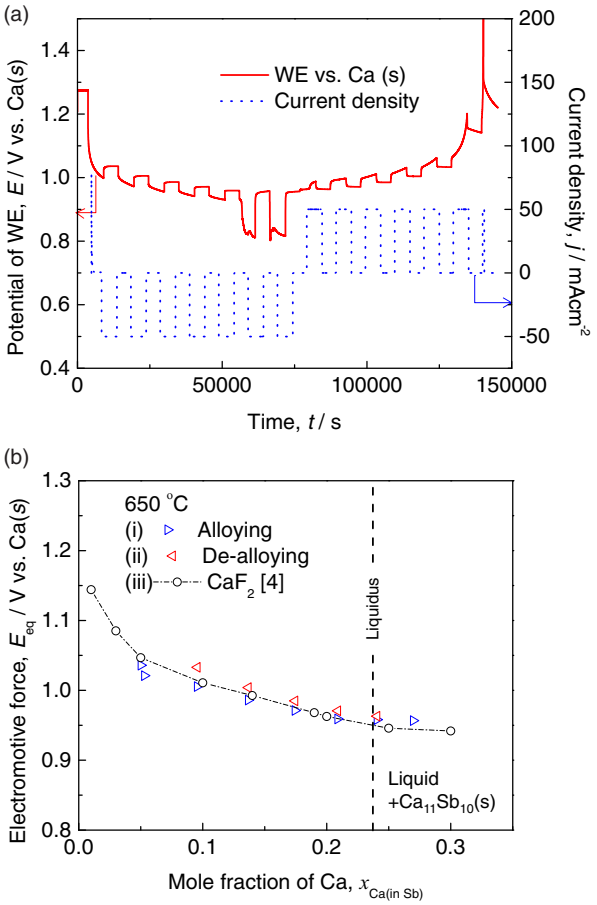


**Figure 3** (a) Potential of the WE and current density during the measurement in the coulometric titration at 650°C, (b) $E_{eq}$ values of the WE as a function of composition of the Ca-Sb electrode at 650°C; (i) the $E_{eq}$ values at each alloying step are forward facing triangles, (ii) the $E_{eq}$ values at each dealloying step are backward facing triangles, and (iii) the *emf* values measured using $CaF_2$ solid electrolyte are white circles.

WE, $E_{eq}$, in Table I are shown as triangles. The cut-off voltages were set in each test at the value at which the electrode potential drops dramatically. As the current density increased, so did the overpotential of the WE, while $x_{Ca(in\ Sb)}$ at the cut-off voltage decreased. These are the limiting factors of electrode performance, which will be also discussed subsequently.

**Table I. Equilibrium potentials of Ca-Sb alloys [in V versus Ca(*s*)] from coulometric titration (this work) and previously reported *emf* values obtained using $CaF_2$.[4]**

| | 650°C | | 700°C | |
|---|---|---|---|---|
| *x*Ca | This work | Ref. 4 | This work | Ref. 4 |
| 0.05 | 1.04 | 1.05 | 1.03 | 1.05 |
| 0.10 | 1.02 | 1.01 | 1.00 | 1.01 |
| 0.14 | 1.00 | 0.99 | 0.99 | 1.00 |
| 0.17 | 0.97 | - | 0.97 | - |
| 0.19 | - | 0.97 | - | 0.97 |
| 0.20 | - | 0.96 | - | 0.96 |
| 0.21 | 0.96 | - | 0.96 | - |
| 0.24 | 0.96 | - | 0.95 | - |
| 0.25 | - | 0.95 | - | 0.94 |
| 0.27 | 0.96 | - | 0.93 | - |
| 0.30 | - | - | - | 0.94 |

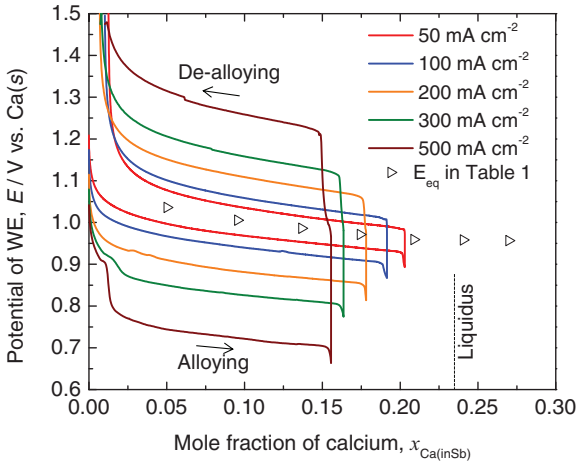


**Figure 4** The potential of the WE, $E$, measured as a function of current density during continuous alloying and dealloying of Ca with the Sb electrode and the $E_{eq}$ values in Table I at 650°C.

*Coulombic efficiency.*—Coulombic efficiency can be defined under constant current density as

$$\eta_Q = 100\left(\frac{t_a\,|-j|}{t_d\,|j|}\right), \qquad [11]$$

where $t_a$ is the time of alloying, $t_d$ the time of dealloying, and $j$ the current density at the surface of the electrode (electrode/electrolyte interface). Figure 4 shows that the so-defined round-trip coulombic efficiencies, $\eta_Q$, of Ca-Sb electrodes are estimated to be 100–104% at current densities of 50–500 mA cm$^{-2}$. Loss of coulombic efficiency can be caused by electronic current through the electrolyte and dissolution of electrode materials in the electrolyte. The chemical consumption can originate from the solubility of calcium metal in the electrolyte as subvalent species ($Ca_2^{2+}$ or $Ca^+$)[7] or from the solubility of Ca-Sb alloy in the molten salt electrolyte as ionic species (e.g., $Ca^{2+}$ and $Sb^{3-}$), as has been observed with Li- and Na-based alloys.[15,16] Electronic conductivity in the electrolyte depends upon the solubility of Ca metal.[17] In our set-up with Ca-Bi as CE, the activity of Ca in Sb is lower than in Bi, providing a chemical short-circuit of Ca from Bi CE to Sb WE, leading to self-discharge of the WE. In contrast, the chemical dissolution of Ca-Sb alloys as ionic species can cause the loss of Sb WE, particularly on deep discharge, leading to coulombic capacity loss. This can result in apparent coulombic efficiency exceeding 100% during the subsequent dealloying process.

The self-discharge current densities, $-j_s$, were measured at 650°C while holding at discrete electrode potentials between 0.95 V and 1.48 V for 12 h, Figure 5. At electrode potentials over 1.02 V, dealloying current (Ca removal) flows due to the chemical transport of Ca into the WE. In contrast, alloying current (Ca deposition) flows at electrode potentials below 1.02 V ($x_{Ca(in\ Sb)} > 0.10$), possibly due to the dissolution of Ca-Sb alloys into the electrolyte. Okada et al. found that the solubility of Sb from a Na-Sb alloy into a sodium halide melt increased as the Na concentration in the Na-Sb alloy increased.[16]

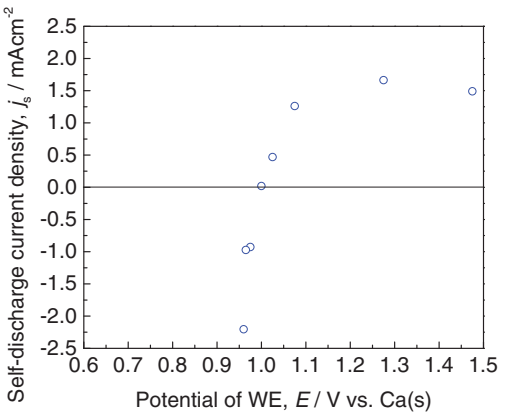


**Figure 5** Self-discharge current densities, $j_s$ at different electrode potentials at 650°C.

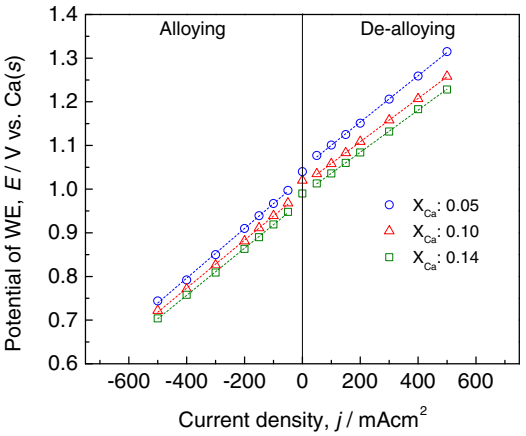


**Figure 6** The potential of WE and the $E_{eq}$ values as a function of current density at 650°C at $x_{Ca(in\ Sb)} = 0.05$, 0.10, and 0.14. The $R^2$ values of the lines were greater than 0.999.

*Dependence of overpotential on current density.*—The electrode potential, $E$, differs from the equilibrium electrode potential, $E_{eq}$, as follows:

$$E(j) = E_{eq} - \eta_{tot}(j) - \eta_{self}, \qquad [12]$$

where $\eta_{tot}(j)$ is total overpotential, which is current density dependent and can be written by

$$\eta_{tot}(j) = \sum_i \eta_i(j) = \eta_{ohm}(j) + \eta_{ct}(j) + \eta_{mt}(j), \qquad [13]$$

where $\eta_{ohm}$ is an ohmic overpotential, $\eta_{ct}$ a charge transfer overpotential, and $\eta_{mt}$ a mass transport overpotential. $\eta_{self}$ is an overpotential due to the self-discharge current, which is not dependent on the current density.

To estimate the total overpotential, $\eta_{tot}$, the electrode potential of the WE, $E$, during the continuous alloying and dealloying processes and the equilibrium potentials of the WE, $E_{eq}$, obtained from the titration experiment at $x_{Ca(in\ Sb)} = 0.05$, 0.10, and 0.14 are plotted as a function of current density in Figure 6. Least-squares fits of the electrode potentials at $x_{Ca} = 0.05$, 0.10, and 0.14 during alloying and dealloying are drawn in Figure 6. The calculated area specific total resistivities, $A \cdot R_{tot}$, are listed in Table II. The area specific ohmic resistance $A \cdot R_{ohm}$ at $x_{Ca(in\ Sb)} = 0.05$, 0.10, and 0.14 was measured by EIS. Results are listed in Table II. As is typical for a three-electrode setup, the area specific ohmic resistance $A \cdot R_{ohm}$ contribution was small ($\sim 0.07\ \Omega\ cm^2$), about 10% of the area specific total resistance $A \cdot R_{total}$. The ohmic overpotential, $\eta_{ohm}$, varies linearly with current density; therefore, the linear correlation of the electrode potential up to 500 mA cm$^{-2}$ in Figure 6 and Table II indicates that the charge transfer resistance, $R_{ct}$, and mass transport resistance, $R_{mt}$, are small

**Table II. The area specific total resistance, $A \cdot R_{tot}$, the ohmic resistance, $A \cdot R_{ohm}$ at 650°C.**

| $x_{Ca(in\ Sb)}$ | $A \cdot R_{tot}/\Omega\ cm^2$ | $A \cdot R_{ohm}/\Omega\ cm^2$ |
|---|---|---|
| 0.05 | 0.57 | 0.07 |
| 0.1 | 0.55 | 0.07 |
| 0.14 | 0.54 | 0.07 |

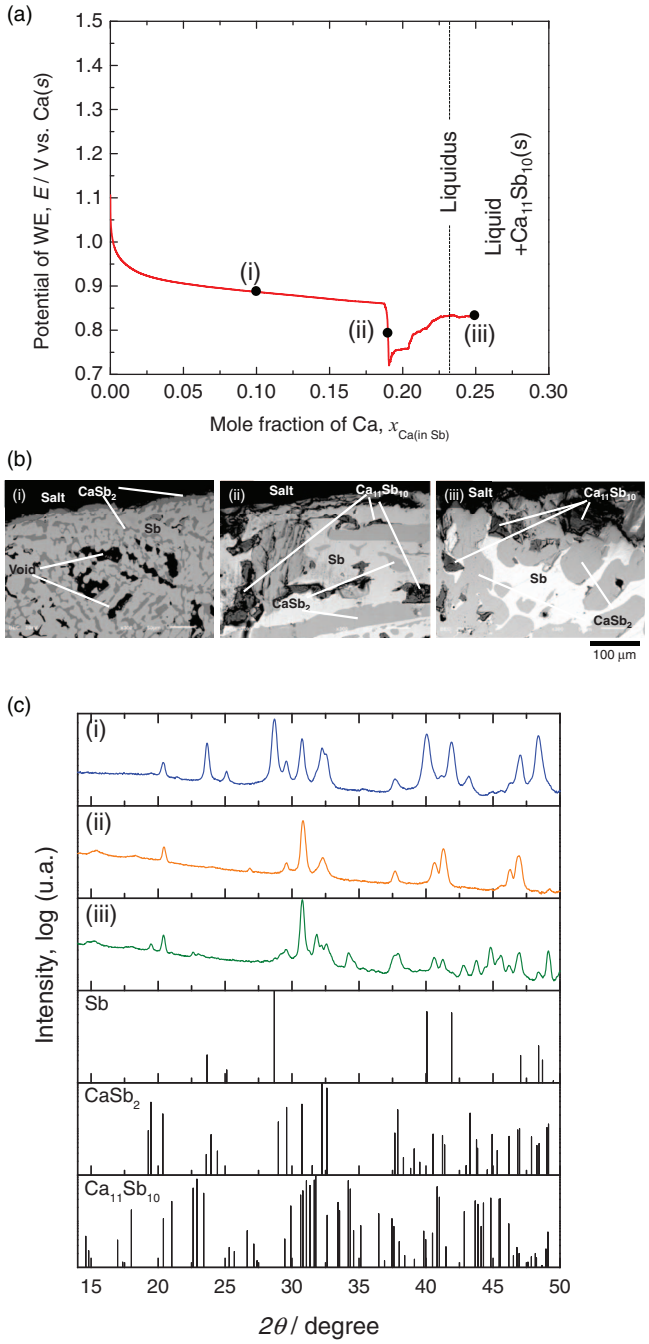


**Figure 7** (a) The potential of the WE, $E$, measured during continuous alloying of Ca with the Sb electrode at a current density of 200 mA cm$^{-2}$ at 650°C, (b) The cross-sectional SEM images of the electrode/electrolyte interfaces, and (c) X-ray diffraction patterns collected on the top of WEs: (i) $x_{Ca} = 0.10$, (ii) $x_{Ca} = 0.18$, and (iii) $x_{Ca} = 0.25$. Samples are covered with petroleum jelly to avoid oxidation for XRD.

enough to enable linear approximation of the overpotential of charge transfer, $\eta_{ct}$, and mass transport, $\eta_{mt}$ versus current density, $j$.

*Formation of intermetallic compounds.*—The alloying process was analysed in detail by SEM and XRD to reveal the reason for the drop-off in potential, which was expected due to the formation of an intermetallic Ca-Sb compound with the attendant decrease in chemical potential of Ca. Three different WEs were prepared at 650°C, current density of 200 mA cm$^{-2}$, stopping at $x_{Ca(in\ Sb)} = 0.10$, 0.18, and 0.25 as shown in Figure 7a. The cross-sectional SEM images and XRD patterns of the electrodes after cooling are shown in Figure 7b SEM, and Figure 7c XRD: (i) $x_{Ca} = 0.10$, (ii) $x_{Ca} = 0.18$, and (iii) $x_{Ca} = 0.25$. Although these data are obtained from the samples after cooling, one can see dramatic differences in phase morphology between the different electrodes, which suggests the formation of new phases during alloying. The densities and the crystal structures of Ca-Sb alloys and compounds are summarized in Table III.

Calcium was highly concentrated on the top of the electrode during discharging. In addition, the higher-calcium-ratio intermetallics were expected to float and were observed on the top of the positive electrode owing to their lower densities. Accordingly, the XRD data were collected from the top of the electrodes to capture the signals from the high-calcium intermetallics. On the electrode at $x_{Ca} = 0.10$ rhombohedral Sb was observed in the SEM image in Figure 7(b, i) and XRD pattern in Figure 7(c, i) as well as the monoclinic $CaSb_2$ phase, which is expected to be formed during the cool down, based on the phase diagram in Figure 2. A phase with acicular structure is observed in the electrode at the drop-off mole fraction ($x_{Ca} = 0.18$). From the SEM image in Figure 7(b, ii) this needle-like phase is confirmed to be $CaSb_2$. On the top of the electrode in Figure 7(b, ii), a $Ca_{11}Sb_{10}$ high-melting solid intermetallic phase is observed. This was also confirmed by XRD data in Figure 7(c, ii). Based on the phase diagram in Figure 2 this compound should not form, suggesting that there was a zone of highly concentrated Ca at the surface of the electrode generated by passing excessively high current. The electrode with $x_{Ca} = 0.25$ exhibits a higher concentration of $Ca_{11}Sb_{10}$ phase based upon SEM in Figure 7(b, iii) and XRD in Figure 7(c, iii). The peaks associated with $Ca_5Sb_3$, $Ca_2Sb$, and Ca phases were not observed.

Based upon these results, the nucleation of the $Ca_{11}Sb_{10}$ phase is thought to be the reason for the drop-off in potential seen in Figure 3a, Figure 4, and Figure 7a. Since the potential of the WE is unsettled at Ca concentrations higher than that of nucleation in Figure 7a, we defined the capacity of the system by the mole fraction of calcium at which the nucleation of the $Ca_{11}Sb_{10}$ phase occurs. Furthermore, the decrease in capacity with increasing current density is attributed to accumulation of Ca at the surface of the electrode. In other words, at high current density the rate of production of elemental Ca at the electrode surface (by transport of $Ca^{2+}$ ions and their reduction to elemental Ca by charge transfer) exceeds the rate of dissipation of elemental Ca in the Ca-Sb alloy pool.

The effect of temperature on alloying and dealloying of Ca with Sb was evaluated. The potentials of the WEs during alloying at 650°C and 700°C at different current densities are compared in Figure 8a–8f. The equilibrium potentials of the WE, $E_{eq}$, are also shown in Figure 8g, and 8h by way of comparison. The differences in equilibrium potential are small (< 0.01 V); however, the effect of the iR drop in the electrolyte is clearly observable in the value of potential difference between 650°C and 700°C. As temperature increases, the solubility of Ca in the Sb electrode increases, even when the nucleation of $Ca_{11}Sb_{10}$ occurs, and approaches the liquidus (theoretical solubility) of the phase diagram in Figure 2. We attribute this to the increase in diffusion in the intermetallic with temperature. Put another way, the high operating temperature enhances the capacity of the Ca-Sb system. The plateau and step appearing at high current densities (> 300 mA cm$^{-2}$) at 650°C around $x_{Ca(in\ Sb)} = 0.01$ were not observed at 700°C at current densities as high as 500 mA cm$^{-2}$. This may be due to the presence of an intermetallic compound formed by codeposition of Li and Na. The high solubility of the intermetallic at high temperature may avert the plateau and step.

*Cycling performance of alloying and dealloying.*—To evaluate the cycling performance of the cell, it was charged and discharged at a current density of 200 mA cm$^{-2}$ at both 650°C and 700°C. The cut-off voltage was set at 0.84 V vs. Ca(s) to prevent intermetallic formation and dissolution of Ca-Sb. The effect of cycling on the alloying, $Q_a$, and dealloying, $Q_d$, capacities is shown in Figure 9. Based on the value of the solubility of Ca in the Ca-Sb alloy from the phase diagram in Figure 2, the theoretical capacity of the cell was estimated to be 0.124 Ah at 650°C and 0.136 Ah at 700°C. The coulombic efficiencies, $\eta_Q$, of the alloying and dealloying processes were determined to be 100% at 650°C and 102% at 700°C. As an indication of the high degree of

**Table III. Densities and crystal structures of Ca-Sb alloys.**

| Phase | $x_{Ca}$ | T/K | Density, ρ / g cm$^{-3}$ | Space group (Pearson symbol) | Lattice parameter nm | Lattice parameter degrees | Refs. |
|---|---|---|---|---|---|---|---|
| Sb | 0.00 | 298 | 6.72 | $R\bar{3}$m (hR6) | a = 0.43056<br>b = 0.43056<br>c = 1.125 | α = 90<br>β = 90<br>γ = 120 | 18 |
| $CaSb_2$ | 0.33 | 298 | 5.45 | $P12_1/m1$ (mP6) | a = 0.4746<br>b = 0.4177<br>c = 0.89913 | α = 90<br>β = 104.14<br>γ = 90 | 19 |
| $Ca_{11}Sb_{10}$ | 0.52 | 298 | 4.44 | $14/mmm$ (tI84) | a = 1.194<br>b = 1.194<br>c = 1.74 | α = 90<br>β = 90<br>γ = 90 | 20 |
| $Ca_5Sb_3$ | 0.63 | 298 | 3.79 | $P6_3/mcm$ (hP16) | a = 0.90312<br>b = 0.90312<br>c = 0.70254 | α = 90<br>β = 90<br>γ = 120 | 21 |
| $Ca_2Sb$ | 0.67 | 298 | 3.78 | $14/mmm$ (tI12) | a = 0.467<br>b = 0.467<br>c = 1.628 | α = 90<br>β = 90<br>γ = 90 | 22 |
| (Ca) rt | 1.00 | 298 | 1.53 | $Fm\bar{3}m$ (cF4) | a = 0.5582<br>b = 0.5582<br>c = 0.5582 | α = 90<br>β = 90<br>γ = 90 | 23 |
| (Ca) ht | 1.00 | 740 | 1.48 | $Im\bar{3}m$ (cI2) | a = 0.448<br>b = 0.448<br>c = 0.448 | α = 90<br>β = 90<br>γ = 90 | 24 |

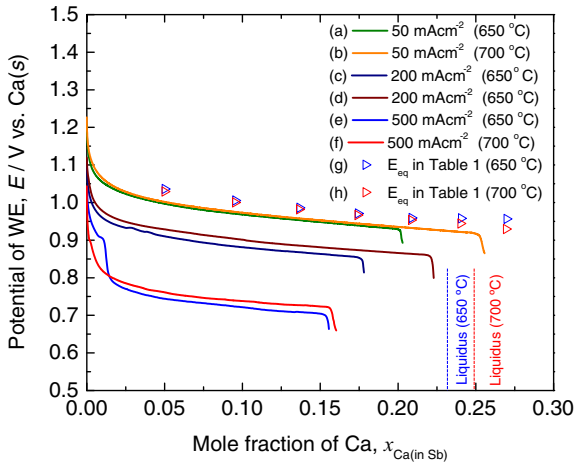


**Figure 8** Potentials of WEs during the alloying and dealloying processes of Ca with Sb at 650°C and at 700°C and $E_{eq}$ values in Table I obtained in this study; temperatures are (a, c, e) 650°C and (b, d, f) 700°C; current densities are (a, b) 50 mA cm$^{-2}$, (c, d) 200 mA cm$^{-2}$, and (e, f) 500 mA cm$^{-2}$.

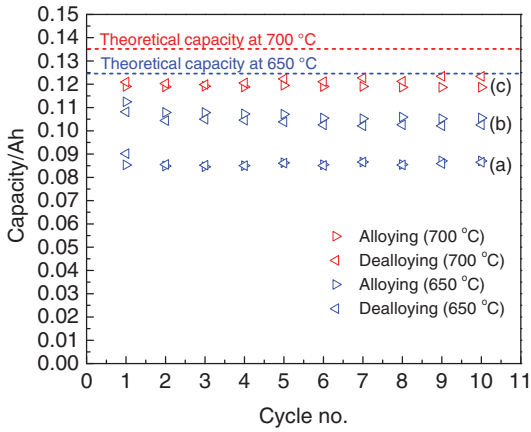


**Figure 9** The capacities of the alloying and dealloying processes with the progression of cycles. Temperatures were (a, b) 650°C and (c) 700°C. Current densities were (a, c) 200 mA cm$^{-2}$ and (b) 50 mA cm$^{-2}$. The theoretical capacity at 650°C and at 700°C calculated based on the phase diagram [8] were 0.124 Ah and 0.136 Ah, respectively.

bi-directionality of the alloying/dealloying reactions and of the long-term sustainability of the cell, the capacity fade rate was measured to be less than 0.01% cycle$^{-1}$, even with the dissolution of Ca-Sb in electrolyte. This means that most of dissolved $Sb^{3-}$ was regenerated into the WE within the potential window of alloying (discharge) and dealloying (charging) as in the ambipolar cell.[25]

*Cost estimation.*— Based upon the market prices of Ca (0.14 $ mol$^{-1}$)[26] and Sb (1.18 $ mol$^{-1}$)[27]combined with the available thermodynamic data, the energy cost of the Ca-Sb alloy was estimated to be 69 $ kWh$^{-1}$ at 700°C. This assumed no dependence in performance on current density. In this study, the nominal cell voltage at 200 mA cm$^{-2}$ was measured to be 0.90 V at 650°C and 0.91 V at 700°C, while the solubility of Ca in the Ca-Sb alloy, $x_{Ca}$, was measured to be 0.18 at 650°C and 0.22 at 700°C. The estimated electrode cost of a Ca||Sb cell operating at a current density of 200 mA cm$^{-2}$ charging and discharging is 114 $ kWh$^{-1}$ at 650°C and 90 $ kWh$^{-1}$ at 700°C, which make this system attractive for grid-level energy storage.

## Conclusions

The electrochemical properties of the Ca-Sb electrode in LiCl-NaCl-$CaCl_2$ multi-cation electrolyte were evaluated. The solubility of Ca from a liquid Ca-Sb electrode was observed to be quite small in the multi-cation molten salt electrolyte, as evidenced by the small *emf* difference between this study and one employing a solid $CaF_2$ electrolyte. The Sb electrode shows good cycling performance (current density over 50–500 mA cm$^{-2}$ with cell voltage tracking over 0.95–0.75 V) at high coulombic efficiency (~100%), and small capacity fade (< 0.01% cycle$^{-1}$), at low capital cost (90 $ kWh$^{-1}$).

## Acknowledgment

The authors are grateful for the financial support of the US Department of Energy, Advanced Research Projects Agency-Energy

(Award No. DE-AR0000047), Total, S.A., Marubun Research Promotion Foundation, and Murata Overseas Scholarship Foundation.

## References


1. D. J. Bradwell, H. Kim, A. H. C. Sirk, and D. R. Sadoway, *J. Am. Chem. Soc.* **134**(4), 1895 (2012).
2. H. Kim, D. A. Boysen, J. M. Newhouse, B. L. Spatocco, B. Chung, P. J. Burke, D. J. Bradwell, K. Jiang, A. A. Tomaszowska, K. Wang, W. Wei, L. A. Ortiz, S. A. Barriga, S. M. Poizeau, and D. R. Sadoway, *Chem. Rev.* **113**, 2075 (2013).
3. P. C. K. Vesborg and T. F. Jaramillo, *RSC Advances* **2**(21), 7933 (2012).
4. S. Poizeau, H. Kim, J. M. Newhouse, B. L. Spatocco, and D. R. Sadoway, *Electrochim. Acta* **76**, 8 (2012).
5. R. A. Sharma, *J. Phys. Chem.* **74**(22), 3896 (1970).
6. J. M. Newhouse, S. Poizeau, H. Kim, B. L. Spatocco, and D. R. Sadoway, *Electrochim. Acta* **91**, 293 (2013).
7. H. Kim, D. A. Boysen, T. Ouchi, and D. R. Sadoway, *J. Power Sources* **241**, 239 (2013).
8. H. Okamoto, Ca-Sb Phase Diagram, ASM Alloy Phase Diagrams Center, P. Villars, editor-in-chief; H. Okamoto and K. Cenzual, section editors; http://www1.asminternational.org/AsmEnterprise/APD, ASM International, Materials Park, OH, 2006.
9. C. J. Wen, B. A. Boukamp, R. A. Huggins, and W. Weppner, *J. Electrochem. Soc.* **126**(12), 2258 (1979).
10. H. Kim, D. A. Boysen, D. J. Bradwell, B. Chung, K. Jiang, A. A. Tomaszowska, K. Wang, W. Wei, and D. R. Sadoway, *Electrochim. Acta* **60**, 154 (2012).
11. A. S. Dworkin, H. R. Bronstein, and M. A. Bredig, *J. Phys. Chem.* **70**(7), 2384 (1966).
12. H. A. Laitinen, R. P. Tischer, and D. K. Roe, *J. Electrochem. Soc.* **107**(6), 546 (1960).
13. A.D. Pasternak and D. R. Olander, *AIChE. J.* **13**(6), 1052 (1967).
14. G. J. Janz and N. P. Bansal, *J. Phys. Chem. Ref. Data* **11**(3), 505 (1982).
15. M. S. Foster, in *Regenerative EMF Cells*, 64, p 136, American Chemical Society (1967).
16. M. Okada, R. A. Guidotti, and J. D. Corbett, *Inorg. Chem.* **7**(10), 2118 (1968).
17. A. S. Dworkin, M. A. Bredig, and H. R. Bronstein, *Discuss. Faraday Soc.* 32, 188 (1961).
18. W. S. Kim, *J. Alloys Compd.*, **252**, 166 (1997).
19. K. Deller and B. Eisenmann, *Z. Anorg. Allg. Chem.*, **425**, 104 (1976).
20. K. Deller and B. Eisenmann, *Z. Naturforsch. B*, **31**, 29 (1976).
21. E. A. Leon Escamilla and J. D. Corbett, *Chem. Mater.*, **18**, 4782 (2006).
22. B. Eisenmann and H. Schäfer, *Z. Naturforsch. B*, **29**, 13 (1974).
23. G. Bruzzone, *Boll. Sci. Fac. Chim. Ind. Bologna*, **24**, 113 (1966).
24. B. T. Bernstein and J. F. Smith, *Acta Crystallogr.*, **12**, 419 (1959).
25. D. J. Bradwell, S. Osswald, W. F. Wei, S. A. Barriga, G. Ceder, and D. R. Sadoway, *J. Am. Chem. Soc.* **133** (49), 19971 (2011).
26. Alibaba http://www.alibaba.com (accessed in 2014 June).
27. MetalPrices.com http://www.metalprices.com (accessed in 2014 June).